Highly Reproducible Physiological Asymmetric Membrane with Freely-Diffusing Embedded Proteins in a 3D-Printed Microfluidic Setup

Paul Heo, Sathish Ramakrishnan, Jeff Coleman, James Rothman, Jean-baptiste Fleury, Frederic Pincet

Highly Reproducible Physiological Asymmetric Membrane with Freely-Diffusing Embedded Proteins in a 3D-Printed Microfluidic Setup

Paul Heo, Sathish Ramakrishnan, Jeff Coleman, James E. Rothman, Jean-Baptiste Fleury,* and Frederic Pincet**

Dr. P. Heo, S. Ramakrishnan, Prof. F. Pincet
Laboratoire de Physique de l'Ecole Normale Supérieure,
PSL Research University
CNRS
Sorbonne Université
Université Sorbonne Paris Cité
Paris 75005, France
E-mail: pincet@lps.ens.fr

Dr. S. Ramakrishnan, J. Coleman
Department of Cell Biology
Yale School of Medicine
Connecticut 06510, USA

Prof. J. E. Rothman
Ecole Normale Supérieure
PSL University
75005 Paris, France
E-mail: james.rothman@ens.fr

Dr. JB. Fleury
Department of Experimental Physics and Center for Biophysics
Saarland University
Saarbruecken D-66123, Germany
E-mail: jean-baptiste.fleury@physik.uni-saarland.de

Keywords: horizontal free-standing bilayer, oriented protein insertion, fluorescence recovery after photobleaching, 3D-printing, microfluidic chip

Abstract

Experimental setups to produce and to monitor model membranes have been successfully used for decades and brought invaluable insights into many areas of biology. However, they all have limitations that prevent the full *in vitro* mimicking and monitoring of most biological processes. Here, a suspended physiological bilayer-forming chip is designed from 3D-printing techniques. This chip can be simultaneously integrated to a confocal microscope and a path-clamp amplifier. It is composed of poly(dimethylsiloxane) (PDMS) and consists of a ~100 µm hole, where the horizontal planar bilayer is formed, connecting two open crossed-channels which allows altering each lipid monolayer separately. The bilayer, formed by the zipping of two lipid leaflets, is free-standing, horizontal, stable, fluid, solvent-free and flat with the 14 types of physiologically relevant lipids and the bilayer formation process is highly reproducible. Because of the two channels, asymmetric bilayers can be formed by making the two lipid leaflets of different composition. Furthermore, proteins, such as transmembrane, peripheral, and pore-forming proteins, can be added to the bilayer in controlled orientation and keep their native mobility and activity. These features allow *in vitro* recapitulation of membrane process close to physiological conditions.

1. Introduction

As the boundary between two regions, biological membranes are the active location where many biological processes occur, including molecular reactions and signal exchanges. Lipids are the main building blocks of membranes and their self-assembly through non-covalent interaction confers adjustable and adaptable properties to the membrane. One key feature of biological membranes is that they are asymmetric, *i.e.* the two lipid leaflets contain different types and distributions of lipids. This asymmetry allows processes to take place specifically on either side of the membrane. Also, the surrounding aqueous environment of each membrane, *e.g.* the local composition of the cytosol, is very dynamic and often changes rapidly to drive each biological process.

It has long been recognized that *in vitro* model membranes help to characterize and understand these various exchanges and reactions at the membrane level. To be as close as possible to physiology, model membranes have to be fluid, and asymmetric with relevant compositions of lipids and proteins for each leaflet. In addition, reproducing reactions that occur at the membrane level necessitates that the surrounding medium on either side of the membrane be quickly adjustable. Finally, for their complete monitoring, model membranes must be compatible with both conventional electrical and optical observation which requires that they are large enough, typically ~100 μm^2 or more, horizontal, and stable over more than 1 hour. All these criteria have to be simultaneously met in a single setup to *in vitro* recreate a physiological membrane and to properly interpret membrane processes.

Currently used model membranes are either supported[1-3] or free-standing[4-12] lipid bilayers. Supported bilayers are usually formed by spreading vesicles on mica, glass, or Si/SiO_2. They offer a relatively stable platform and can be asymmetric. However, they present membrane imperfections, defective mobility of lipids and transmembrane proteins due to interactions with the underlying substrate, and there is no direct access to the space between the membrane and the substrate. Because of these limitations, free-standing membranes have been gaining

popularity as they satisfy some of the fundamental criteria: they are fluid and both sides are in contact with the aqueous medium. Historically, vesicles[4, 5, 13] and black lipid membranes[6] were among the first suspended membranes to be successfully used. Over the years, many setups have been developed that provide multiple ways to form suspended membranes, *e.g.* on a hole between two separate compartments,[7, 14] at the tip of pipettes,[8, 9, 15] between two emulsion droplets,[10] on holey substrates,[11, 16] on nanodiscs,[12, 17, 18] and in microfabricated systems.[19-23] Some of the other criteria are difficult to achieve with these suspended systems. One common difficulty is to recreate asymmetric bilayer. Their preparation often leads to the inclusion of an organic solvent layer that affects the biophysical properties of the membrane and they are extremely limited in terms of lipid composition.[13, 24-26] Also, the stability of the bilayers is often an issue which is resolved in the vast majority of planar bilayer setups by using a non-physiological lipid, DPhPC (1,2-diphytanoyl-sn-glycero-3-phosphocholine).[19, 20, 27] DPhPC is relatively adapted to study some biological processes like protein channel opening and closing.[28] On the other hand, it has critical limitations that hinder its broader application to mimic physiological membranes, *e.g.* altered protein mobility, absence of lipids or protein domains, lack of local interaction between lipid and proteins.[29, 30] Nevertheless, any criteria regarding the composition, the fluidity, the accessibility, the stability, and the monitoring can be met by one of the existing setups. However, a current limitation to the actual replication of physiological processes is that no technique can simultaneously validate all these criteria (see Supporting Note and Table S1, Supporting Information, for their detailed description and comparison). Hence, a critical challenge is to obtain a system that validates all the criteria.

Here, we address this question by introducing a straightforward setup to form and monitor a horizontal free-standing lipid bilayer fulfilling all the requirements to mimic physiological membranes, notably making it stable, flat, asymmetric and with a physiological composition (**Figure 1**). This method is inspired by four observations. First, only microfluidic devices having at least two accessible channels facing each lipid monolayer allow quick changes of the

medium in both sides of the bilayer without disturbing the fragile membrane. Second, to be observable under a microscope, the membrane must be horizontal. Third, 3D-printing techniques can be used to manufacture highly versatile bilayer-forming devices that are adaptable to any monitoring equipment, such as microscope or patch-clamp amplifier. Fourth, in most current systems, the general principle to successfully make free-standing membranes is to start from two monolayers separated by oil and subsequently drain the oil so that the monolayers contact and form a bilayer. During this process, the drainage phase leaves an annulus of oil and possibly the presence of an oil film between the two lipid monolayers. To significantly reduce the amount of residual oil, Malmstadt et al. introduced the principle of automated lipid bilayer formation, *i.e.* without any external triggering, in poly(dimethylsiloxane) (PDMS) chip by selective solvent extraction.[31] These four observations led us to design a single-block dual-channels PDMS microfluidic chip made from 3D-printed molds to form and monitor horizontal membranes. The chip is integrated with a spinning-disk confocal microscope and a path-clamp amplifier to observe the bilayer formation and following processes synchronously. Concurred observations indicate that the bilayer is free-standing, stable, large, solvent-free, fluid and flat, even when having a physiological composition. The aqueous medium adjacent to both sides of the membrane can be readily changed, allowing the membrane to be asymmetric and proteins to be present on either side of the membrane with controlled orientation and full functionality.

2. Results

First, the chip fabrication, from 3D-printing to single-block microfluidic chip, is described. Then, as a proof of concept for the physiological-like membrane, we present the following: strategies to form symmetric or asymmetric membranes, characterization of asymmetry, stability, flatness, and fluidity of the bilayer, versatility of the setup to make a correctly oriented protein on either side of the membrane, and finally protein functionality verification.

2.1. Design, 3D-printing, and fabrication of the chip

The device presented here is mainly composed of PDMS which was poured on 3D-printed molds (Figure 1 and Figure S1a, Supporting Information). The PDMS chip contains two horizontal crossed-channels connected by a hole. During the membrane formation process, a squalene droplet is initially trapped in this hole and separates the two channels. A lipid monolayer is formed on each side of the squalene droplet. Squalene is absorbed by PDMS which brings the two monolayers spontaneously into contact, and the free-standing bilayer having a horizontal geometry starts to form in the hole.

2.1.1. Chip geometry and 3D-printing

Two molds are produced with a tabletop high-resolution digital light processing (DLP) / Stereolithography (SLA) 3D-printer (Figure 1, and Figure S1b-d, Supporting Information). The bottom mold provides the shape of the bottom channel that will be located between the cover glass and PDMS. The channel dimensions are: 10 mm x 400 µm x 200 µm (length x width x height). The top mold has the shape of the top channel (5 mm x 400 µm x 200 µm, length x width x height) and a ~100 µm diameter height cylinder of radius ~50 µm located at its center. This cylinder, that can easily be of other shapes by 3D-printing (*e.g.* triangular or rectangular, Videos SV1-3, Supporting information), will produce the hole between the two channels. The two molds are assembled and the final structure is ready to be filled with PDMS (see Experimental Section for details).

2.1.2. PDMS chip fabrication

PDMS was poured into the assembled top and bottom molds. When the cured PDMS was detached from the molds, the chip is a single-block PDMS containing two grooves that need to be sealed to form channels. An additional PDMS cube having inlet and outlet holes is used to

cover the top channel. A second PDMS cube is attached to the bottom inlet part, both inlet and outlet holes were punched, and finally bottom channel was created by plasma bonding with coverslip (Figure 1, and Figure S1a, Supporting Information, see Experimental Section for details).

2.2. Horizontal free-standing membrane formation

In vitro bilayer reconstitution in the microfluidic chip is a three steps procedure: trapping a squalene droplet in the hole between the two channels, spreading a lipid monolayer at the squalene/buffer interface and spontaneous removal of the squalene by PDMS.

2.2.1. Suspending a nanoliter squalene droplet in the hole

Initially, the chip is filled up with squalene, aqueous buffer is flowed in and pushes the oil away in the bottom channel first and in the top channel right after. The oil in the hole is not affected by these two buffer flows, leaving a 70-100 μm thick oil droplet (~1 nL volume) suspended between the two channels (**Figure 2**a). As a result, an oil/buffer interface is facing each channel. These interfaces are highly reactive because they have a high surface tension, typically a few mN/m.

2.2.2. Sandwiching the squalene droplet between two lipid monolayers

At that point, monolayers need to be spread on both oil/buffer interfaces. Amphiphilic molecules presented in the vicinity of the interface will spontaneously insert their hydrophobic tails in the oil with their polar head facing the buffer to decrease the surface tension. Hence, to make monolayers on squalene droplets, lipids can be brought from either the oil or the aqueous phase. In the following, we compare the two methods.

Lipid-in-oil approach: All the ~2 mg/mL lipids we tested could be resuspended in squalene upon thorough mixing and heating at 50 °C for 30 min, and at 24 °C for 12 hours. Once the lipids/squalene droplet is trapped at the hole, lipids from squalene spontaneously rearrange and form lipid monolayers at both oil/buffer interfaces. Note that, with this protocol, both monolayers necessarily have the same composition. The lipid molecules remaining in the oil phase affect the droplet lifetime and the bilayer flatness. Further details are described in §2.4.1., §2.4.2., and 3. Discussion.

Small unilamellar vesicles-on-oil approach: Since the device presented here has dual open channels, small unilamellar vesicles (SUVs) can be used as a carrier of the lipids. After the squalene droplet is trapped in the hole, SUVs are flowed in each channel and form a monolayer by spontaneously spreading on the squalene/buffer interfaces which are highly reactive. It is important to have enough SUVs in the solution to obtain a sufficient coverage of the interface when the two monolayers contact. If the coverage is insufficient, the bilayer will immediately break. Typically, SUVs with 5 mM lipid concentration are forming finely packed monolayers. Note that the SUVs flowed in the two channels can be of different compositions which gives diversity in each monolayer, *e.g.* asymmetric lipids composition and distribution as well as proteins.

2.2.3. Bilayer formation

As a result of squalene absorption by PDMS, the oil-free region in the center of the squalene phase nucleates a contact of two lipid monolayers, and the bilayer region spreads out over the whole section of the hole upon further absorption.

Kinetics of squalene absorption: In the hole separating the two channels, a lipid-free 1 nL squalene droplet is almost uniformly absorbed by PDMS over the course of ~1 hour (Figure 2d-g). To quantitatively monitor this decrease, we have added a fluorescent dye, BODIPY, in

squalene (Figure 2e). The distance between the two squalene/buffer interfaces decreases in time, slightly faster in the center (Figure 2e-g). When the two lipid-free interfaces meet at the center, the droplet is broken and there is direct contact between the buffers from the two channels as confirmed by the disappearance of any fluorescence in the center (at 70 minutes in Figure 2d) and the simultaneous increase in capacitance to unrealistic values. Note that to prevent useless troubleshooting time, whenever a new chip is fabricated, squalene absorption kinetics was systematically tested. If the absorption time was not ~1 hour, the chip was discarded.

Kinetics of bilayer formation: When there are lipid monolayers at the oil/buffer interfaces, BODIPY-stained squalene shows spontaneous absorption at a similar rate to a lipid-free squalene droplet (Figure 2f,g). The two monolayers get close to each other from the center following the geometric change in lipid-free squalene droplet (**Figure 3**a). The capacitance starts increasing when the fluorescence disappears from the center of squalene droplet (t=80 min, Figure 3a). These simultaneous observations indicate that an oil-free bilayer starts forming at the center of squalene droplet, meaning that the bilayer nucleation is due to the automated thinning process of squalene absorbed by the surrounding PDMS (right panels, Figure 3a). Then, upon further squalene absorption, the bilayer spreads radially in time towards the edge of the hole.

The spreading of the bilayer is synchronously monitored optically in bright-field (Figure 3b) and electrically by capacitance measurement (Figure 3c). Optically, the squalene droplet is initially of relatively uniform intensity. After ~1 hour, a tiny disk briefly appears in the center (at 71 min in the example presented Figure 3b) and is followed, a few seconds later, by a new pattern: a bright and sharp ring suddenly appears indicating a change in refractive index between the two regions of uniform intensity. The bright ring spreads outward and disappears when it coincides with the edge of the hole. To understand the nature of each region delineated by this ring, we have compared the bright-field images with the fluorescence of squalene stained

with BODIPY shown in Figure 3a. There was no visible trace of fluorescence in the inner region surrounded by the ring in bright-field, indicating that the oil was entirely removed from the interspace between the two leaflets. During dilation, the fluorescence overlapped with the outer region of the ring and finally vanished when the ring reached the edge of the hole. Notably, and contrarily to many planar bilayer setups, there is no observable amount of remaining solvent-annulus in a fully extended bilayer.

The simultaneous electric monitoring of the system confirms that the region inside the ring is a zipping bilayer. Initially, the capacitance upon squalene droplet formation is null indicating that the droplet electrically isolates the two channels from each other. When the ring appears (at time 71 min in the example in Figure 3b), a sharp increase in capacitance is observed (Figure 3c). The capacitance continues to increase as the regions delineated by the ring expands (for ~30 min in Figure 3b,c) and plateaus at the end of bilayer expansion. Comparing the area of the expanding disk and the capacitance provides direct information on the bilayer formation and properties (Figure 3d). First, the area of the membrane, observed in bright-field (Figure 3b) or fluorescence (Figure 3a), varies linearly with the capacitance (Figure 3d) as predicted by a dielectric analogy.[32, 33] In addition, the slope of this linear variation gives the value of the specific capacitance of the membrane (~10^{-2} F/m^2) which is consistent with the value reported in the literature for an oil-free bilayer.[34]

All these coinciding results indicate that a horizontal free-standing bilayer is actually formed. The initial transition from no bilayer to a bilayer phase, at 71 min in the example given in Figure 3b-c, takes a couple of seconds. In the first picture (71 min), the ring is dim and the capacitance is still less than 1 pF. A few seconds later (71.1 min), the bright ring suddenly appears and the capacitance continuously increases to 20 pF. This sharp transition can easily be explained. When the squalene layer at the center of the droplet becomes thin enough, a fluctuation brings the two leaflets in close apposition and makes them adhere, forming the nucleation point for the membrane. The adhesion area, *i.e.* the membrane area, increases quickly until the adhesion

energy of the two leaflets is balanced by the internal pressure of squalene. The subsequent increase in area and capacitance is limited by squalene absorption.

A common criticism of the bilayers made from oil is that there may be an oil film trapped between the two leaflets. Even though we showed there is no such film in our setup, we cannot exclude that there are sparse remaining squalene molecules in the bilayer. This is not an issue to mimic biological membrane as tiny amounts of oil molecules coming from (or going to) biological lipid droplets are often physiologically found between the two leaflets and may be very well modeled by these trapped squalene molecules.

2.3. Asymmetric bilayer

Asymmetry is a key feature of physiological membrane that is not often achievable in current model systems.[24-26] Taking advantage of the geometry of the chip, we reproduced the physiological asymmetry of the membrane by forming the lipid monolayers from SUVs having two different compositions in the upper and lower channels respectively (**Figure 4**). To distinguish the two types of SUVs, we labeled their membranes with two different fluorescent dyes. Flowing a quencher of the lower channel lipid dye in the upper channel after bilayer formation did not affect the fluorescence. In contrast, flowing in the same quencher in the lower channel completely removed the fluorescence of the corresponding dye. These results unambiguously show that the membrane is asymmetric and that the lipids in the lower (resp. upper) leaflet come from the SUVs that were flowed in the lower (resp. upper) channel. Also, we did not observe any fluorescence inside the droplet when the squalene is sandwiched between the two monolayers, indicating that the lipid molecules do not spontaneously dissolve in the oil. Finally, there was no significant exchange (flip-flop) between the two leaflets over the lifespan of the membrane (~2 hours).

2.4. General properties of the suspended membrane: stability, shape, and fluidity

To *in vitro* recapitulate a biological process at the membrane, the bilayer made of physiological lipids must be stable long enough, at least for one or two hours, flat enough for optical observation of the reaction over the whole surface and it must be perfectly fluid. We tested these aspects on several symmetric bilayer compositions made from the lipid-in-oil or the SUVs-on-oil approach and two asymmetric membranes.

2.4.1. Stability of the membrane

After the squalene fluorescence signal has disappeared (Figure 3a), the membrane is fully zipped and its area remains constant for a long time until membrane rupture attested by a sudden increase of the capacitance to a non-measurable value. The origin of this rupture can be diverse, but the most likely explanation is that surface tension, which is defined by membrane composition and lipid packing, increases up to the lysis tension. We characterized 14 types of symmetric membranes (both lipid leaflets are the same) with both the lipid-in-oil and SUVs-on-oil protocols and two asymmetric membranes made from SUVs, including one mimicking the composition of physiological plasma membranes (**Figure 5**a). For all cases, the success-rate of membrane formation, *i.e.* the percentage of trials leading to a fully zipped bilayer, was close to 100%. The membrane lifetime, defined as the time difference between membrane formation and lysis, depended on the lipid composition and monolayer formation strategy. Symmetric membranes made from SUVs have a 5 to 55% longer lifetime before lysis than the ones made from lipid-in-oil (Figure 5a). Asymmetric membranes remained intact for almost 3 hours on average which demonstrates this setup is perfectly suited to reproducibly reconstitute stable membranes having physiological lipid composition and asymmetry. Finally, all these membranes are resistant to thorough and repeated replacement of the surrounding buffer (Figure S2, Supporting Information). This resistance to flow shows that the device is appropriate to

reproduce sequential reactions on either leaflet by flowing in reactants in the corresponding channel and that the cylindrical hole probably protects the bilayer from the buffer flow.

Typically, the bilayers presented here have ~100 µm in diameter. We did not systematically evaluate the impact of the hole diameter or shape on the stability. However, the bilayers were successfully formed with diameters ranging from 80 µm to 200 µm. Larger holes (~200 µm) displayed a ~20% faster squalene absorption rate and up to 20% shorter lifetimes. When the hole diameter was less than 80 µm, the bilayer was formed, but the squalene absorption rate was decreased dramatically. As a consequence, in 95% of the cases we tested it took 4 hours or more to form a bilayer which may be limiting for most experimental conditions.

2.4.2. Flatness of the horizontal membrane

In a horizontal bilayer setup, the membrane must be as flat as possible to monitor the entire surface of the membrane in a microscope. In the lipid-in-oil approach, the bilayer is relatively flat and horizontal during the expansion state, but, after full expansion, it often bends which prevents observation in a single confocal image (Figure 5b). In some cases, the membrane grows indefinitely out of the hole as simultaneously attested by optical observation (Video SV6, Supporting Information) and by the capacitance that constantly increases. We assume this increase in area of the bilayer originates from the quasi-infinite supply of lipid in the oil. On the other hand, in the SUVs-on-oil approach, the membrane remains flat and horizontal, making it more suitable for optical observations (Figure 5c). In this method, we never saw the bilayer growing out of the hole, and only in rare case (~10%), the whole membrane is bent similarly to the bilayer formed with lipid-in-oil strategy. We did not observe any significant difference in behavior regarding the flatness of the membrane between the various lipid compositions.

2.4.3. Fluidity

Biological membranes are generally fluid. Free-standing membranes should conceptually be fluid which is not the case with supported bilayers, but the actual mobility of the lipids or proteins is usually not reported for planar bilayer setups. Thus, we decided to extensively investigate the fluidity of the membranes presented here with fluorescence recovery after photobleaching (FRAP) technique (**Figure 6**a-b). In brief, under a scanning confocal microscope, a disk of radius, *r*, is bleached during one frame acquisition by locally increasing the laser power. The total fluorescence recovery over the disk is subsequently monitored in time. This recovery displays a characteristic time, τ. For standard diffusion, τ varies linearly with r^2: $r^2 = 4D\tau$, where D is the diffusion coefficient. We found that τ and r^2 are indeed proportional over a wide range of sizes (10 – 100 µm, Figure 6c). The resulting diffusion coefficient was similar to the one measured on giant vesicles (~10 µm²/s),[35] which is ~2-3 times faster than on supported membranes.[36]

The plateau of the recovery curve also provides relevant information to understand the lipid dynamics in the system. We observed that the intensity of this plateau varied inversely with the size of the disk (Figure 6d). Quantitatively, for a bleached area S_b, the relative plateau intensity, I_p, follows:

$$I_p = \frac{S_t - S_b}{S_t} = 1 - \frac{S_b}{S_t} \qquad (1)$$

where S_t is the total area of the bilayer. Equation (1) is valid when lipid exchange occurs only within the membrane. If other large lipid reservoirs are included, the plateau intensity should always be equal to the pre-bleaching value as all bleached lipids are replaced by fluorescent ones. Since, the variation of the plateau intensity presented in Figure 6d follows exactly the quantitative prediction of Equation (1), the membrane behaves like an isolated entity without any lipid exchange with other lipids reservoirs. Interestingly, this almost ideal fit is observed in the lipid-in-oil approach even when the bilayer is not fully expanded. This shows that there is

no lipid transfer from the oil reservoir to the membrane or from the membrane to the oil reservoir on the timescale of the experiment.

2.5. Insertion and characterization of proteins in the bilayer

Finally, three types of membrane proteins have been investigated: t-SNARE (target membrane – soluble N-ethylmaleimide–sensitive factor attachment protein receptor), α-Synuclein, and α-hemolysin, as representative of transmembrane, peripheral, and channel protein examples, respectively. The controlled orientation, fluidity, and functionality of the protein, as well as the electrical properties of the membrane, are characterized including the methods for inserting such proteins into a bilayer.

2.5.1. A transmembrane protein: t-SNARE

Transmembrane proteins, composed of both hydrophobic and hydrophilic domains, have to be mobile, correctly oriented, and functional in a membrane. Their insertion cannot be achieved following lipid-in-oil approach since hydrophilic domains in the oil create protein aggregation and they seldom recover their native conformation. However, using SUVs-on-oil approach with proteo-SUVs, widely used for decades, is a straightforward way to insert transmembrane protein during the lipid monolayer formation. Proteins can be embedded into SUV membranes using one of the standard methods, then these proteo-SUVs are subsequently flowed in the chip to form one of the monolayers or both, *i.e.* proteins can be freely inserted on either side of the membrane (**Figure 7**a). As an example, we have used t-SNARE which is a protein complex containing a single transmembrane domain (TMD) and a large cytosolic domain (CTD). Upon proteo-SUV spreading on squalene, it is expected that the hydrophilic CTD remains in the buffer while the hydrophobic TMD inserts in the oil. After bilayer zipping CTD cannot cross the bilayer and will only be facing the channel in which the proteo-SUVs were flowed, indicating that, in theory, the orientation of the protein can be controlled. To check this

hypothesis, we have flowed proteo-SUVs only in the top channel and protein-free SUVs in the bottom one. After bilayer formation, a fluorescent primary antibody was injected in the bottom and top channels sequentially. This antibody labeled the membrane only on the side of the channel where the proteo-SUVs were presented (Figure 7b,c), proving the correct orientation of the t-SNAREs. A secondary antibody can also be used to confirm the presence of the protein and indicating that this setup is compatible with immunofluorescence assay (Figure S4, Supporting Information). We have used a fluorescently labeled protein and performed FRAP experiments to check the mobility of the t-SNARE in the membrane. The proportionality between r^2 and τ shows that t-SNAREs movement follows standard free diffusion with a diffusion coefficient of ~4 $\mu m^2/s$ (Figure 6c) of the same order as what was previously measured with giant liposomes and sponge phase.[37] Finally, t-SNAREs are functional as they specifically bind the cytosolic domain of the fluorescently labeled cognate partner, vesicular SNARE (v-SNARE, Figure 7d).

Hence, it is possible to successfully insert transmembrane proteins while keeping their mobility, controlled orientation and functionality in this microfluidic setup.

2.5.2. A peripheral protein: α-Synuclein

Peripheral proteins do not have transmembrane domains but spontaneously bind to a membrane, often through amphipathic helices. They are usually soluble in aqueous buffer, hence, in our system, these proteins can be directly flowed in the channel. As a prototypical example of peripheral protein, we tested α-Synuclein, which participates in the regulation of neurotransmission. It binds to negatively charged membranes where it tends to aggregate (Figure 7e). We have flowed fluorescently labeled α-Synuclein in the upper channel after bilayer formation. The membrane became fluorescent after proteins remaining in the buffer were washed out, showing that α-Synuclein binds onto the membrane. In contrast with t-

SNARE, bleaching experiments did not exhibit significant fluorescence recovery at all disk sizes tested, showing that the protein is immobile (Figure 7f). This is consistent with the known aggregation of the protein on the membrane.[38]

2.5.3. A pore-forming protein: α-hemolysin

Finally, we tested a soluble protein that oligomerizes in a heptamer complex and forms a 1-1.5 nm wide channel-like structure that spans through the membrane. To test whether channels were forming in the membrane, we imposed a voltage difference between the two channels, *U*, and measured the current between the electrodes (Figure 7g). Before adding α-hemolysin, no significant current was observed. A current larger than the noise level was only observed when α-hemolysin was added after bilayer formation and was presenting stepwise increase indicating the sequential open-channel formation (Figure 7h). The diameter of the channel is estimated through the relation $d = 2\sqrt{\frac{l\Delta I}{\pi GCU}}$, where d is the pore diameter, l the length of the channel, ΔI the step increase in Current, G the molar conductivity, C the concentration and U the voltage. Using values from the example in Figure 7g (l ~10 nm, ΔI ~50 pA, G ~10 S/Mm, C = 1 M, U = 50 mV), our measurements indicate that the hemolysin pore is equivalent to a freely conducting pore of 1.2 nm in diameter which is close to the reported value, 1.5 nm.[39] To test that this value did not significantly depend on the voltage, we varied U between – 100 mV and + 100 mV and did not observe any significant variation as attested by the linear variation between the current jump and the applied voltage (Figure 7h).

3. Discussion

In this discussion, we will address two points: the impact of lipid packing in each leaflet on the success-rate of membrane formation and the lifetime of the membrane, and general protocols to insert any type of protein with controlled orientation.

3.1. Impact of lipid packing and surface tension on the stability of the membrane

Successful formation and long lifetime of the membrane are intimately connected to lipid packing, which depends on numbers of parameters. We focused on the need to have conical shape lipids to efficiently form membranes and the impact of cholesterol on the lifetime of the membrane.

3.1.1. Success-rate of membrane formation

The surface tension of a membrane is the macroscopic signature of lipid packing at the molecular level. An increase in surface tension indicates a decrease in lipid packing. However, the change in lipid packing between a tensionless membrane and lysis tension is small, 5 to 10% (Figure S5a, Supporting information).[40] As a result, in our setup, successful membrane formation requires that both monolayers are close to maximum lipid density when they contact upon squalene absorption. Attempts to form bilayers made of 1,2-dioleoyl-sn-glycero-3-phosphocholine (DOPC) confirmed that hypothesis. We tried to make pure DOPC membranes from lipids-in-oil and noticed that, upon flowing buffer inside a chip filled with squalene, large structures containing lipid and squalene appeared near the buffer/squalene interface, locally forming what looks like an emulsion (Figure S5b, Supporting information). Hence, lipids from the monolayer are constantly resuspended in the buffer phase by an emulsification process generating an outward flow of lipids that prevents full packing of the monolayer. This is why the success-rate of membrane formation was extremely low with pure DOPC. In 90% of the cases, the membranes did not even start forming and the two monolayers collapsed upon contact as shown by the capacitance and fluorescence measurements. A similar emulsification process resulting in low success rate also occurred when adding 1,2-dioleoyl-sn-glycero-3-phosserine (DOPS) or cholesterol (2 mixtures, DOPC:DOPS (90:10) and DOPC:DOPS:cholesterol (60:10:30), were tested). Overall, we noticed that having 30% or more conical shaped lipids such as 1,2-dioleoyl-sn-glycero-3-phospoethanolamine (DOPE) prevented emulsification

(Figure 5a) and was thus required to have highly reproducible membrane formation. This is probably because conical shape lipids favor negative curvatures while emulsion droplets have positive curvatures.

3.1.2. Lifetime of the membrane

Once a bilayer is formed, it remains stable during the time required for the surface tension to increase from the initial one to the lysis tension (Figure S5a, Supporting information). Hence, lowering the initial surface tension, *i.e.* increasing initial lipid packing, and/or increasing the lysis tension will make the membrane longer-lived.

The impact of the initial surface tension on the lifetime of the membrane is attested by the comparison between the two approaches to form monolayers. It was previously showed that lipid packing in the lipid-in-oil approach is usually lower than in the SUVs-on-oil protocol,[41] making the initial surface tension higher when lipids come from the oil. As a result, a longer membrane lifetime is observed with the SUVs-on-oil protocol.

Membranes with higher lysis tension are expected to have a longer lifetime. It is well known that cholesterol increases lysis tension because it is a tiny amphiphilic molecule that can fill the hydrophobic gaps between larger lipid molecules.[40] This explains our observation that large amounts of cholesterol make membranes longer lived. Also, addition of sulfatide or cerebroside in the bilayer improves the stability. Even though we do not have direct proof, these two components may act in a similar manner as cholesterol by increasing the lysis tension.

Finally, we cannot ignore the fact that the interactions between the membrane and PDMS may play an important role in the stability. Indeed, rupture could occur at the edge, where the membrane adheres to PDMS. However, if this was the case, the lifetime of the bilayer should be relatively independent of the lipid composition because PDMS/membrane interactions should not vary significantly. Since we observed that the lifetime can change more than 10 fold

with the composition, it is unlikely that the membranes break by detaching from PDMS. Hence, the stability is only determined by the lysis tension.

3.2. General principle for inserting any protein in the membrane

The procedure we presented for α-Synuclein and α-Hemolysin can be used with any soluble protein. However, the transmembrane protein we tested, t-SNARE, is peculiar in the sense that it has only two distinct domains of different hydrophobicity: a hydrophilic region (CTD) and a hydrophobic region (TMD), making it prone to spontaneously insert at an oil/buffer interface together with lipids. Though many transmembrane proteins have a similar amphipathic property as t-SNAREs (one hydrophilic and one hydrophobic domain, I, Figure S6, Supporting information), others are either almost purely hydrophobic (tiny hydrophilic loops connecting their transmembrane domains), such as bacteriorhodopsin (II, Figure S6, Supporting information) or present a triple structure: hydrophilic/hydrophobic/hydrophilic domains, such as LDL-receptor (III, Figure S6, Supporting information). In general, these two types of proteins will also settle down at an oil/buffer interface, but they may have uncontrolled orientations and/or may lose their conformation and lose their functionality. Here, we propose strategies to bring these two protein types back to the case of t-SNAREs. To render amphipathic proteins that are almost purely hydrophobic, a common approach is to add a large hydrophilic domain that is cleaved after insertion at the interface. For instance, a green fluorescent protein would be appropriate and present the advantage of facilitating the monitoring of protein insertion by fluorescence. For the hydrophilic/hydrophobic/hydrophilic proteins, it is slightly more complicated. The protein must first be reduced to a hydrophilic/hydrophobic pre-protein. The second hydrophilic domain must be added, for instance by click chemistry, after the pre-protein is correctly inserted in the membrane. Using these strategies, virtually any type of transmembrane protein can be incorporated in the free-standing bilayer with correct and controlled orientation. In addition, purely hydrophobic peptides could be directly added in

squalene and be trapped between the two leaflets after membrane formation. This protocol may be useful to monitor oil-containing biological processes such as lipid droplet formation.

4. Conclusion

In summary, we simultaneously monitored the formation of *in vitro* physiological asymmetric membrane in a newly developed microfluidic setup combined with optical and electrical apparatus. Using a 3D-printing technique, the PDMS chip with adjustable geometry was successfully produced for reconstitution of horizontal free-standing bilayers. Synchronous observation with a confocal microscope and patch-clamp amplifier allows the characterization of the pre-bilayer state and membrane formation. Coincident results from bright-field, 3D-reconstituted fluorescence images and capacitance reveal that membranes composed of physiological lipids are free-standing, solvent-free, fully fluid like giant vesicles, large, and stable over an hour. With this setup, membranes are formed with a success rate close to 100%. The two freely accessible channels adjacent to the bilayer allow the development of a new strategy, using SUVs as carriers of lipids and transmembrane proteins, to form each membrane leaflet separately. Through this protocol, an asymmetric bilayer was reproducibly formed, the membrane was relatively flat for optical observation. Furthermore, membrane proteins were inserted or presented on the bilayer with a controlled orientation while keeping their mobility and functionality. Hence, this chip is the most advanced platform that satisfies all the criteria required for *in vitro* reconstitution of physiological membranes, and can be widely used to monitor almost any biological process at the membrane. Further improvements to the setup can be envisioned, *e.g.* a perfect control and monitoring of the surface tension which may be a key parameter in some physiological processes. Future developments also include the possibility to recreate not only an *in vivo* membrane itself but also a physiological membrane environment, such as cytoskeleton (*e.g.* actin network), which is the first step towards an artificial cell-on-chip.

5. Experimental Section

3D printing: The molds were printed by DLP / SLA combined tabletop printer, Titan2 HR (Kudo3D). The bottom mold which creates a bottom channel between the cover glass and PDMS and the top mold which creates the top channel and the 100 μm diameter and 100 μm height hole connecting the two channels were sketched with computer-aided design (CAD) software, AutoCAD (Autodesk). The exported lithography files (.stl) of the molds were sliced along the z-axis with 100 μm steps by Creation Workshop software (provided by Kudo3D), generating sets of 46 layers graphic files (.png) with 1920 x 1080 pixels resolution. Each .png files were composed of black or white pixels, and it can be modified with any kind of graphic programs (*e.g.* image J or Paint application in Windows OS). All these files are available in Supporting Files SF1-5, Supporting Information. Each set of layer graphics was uploaded into the Titan2 HR. Two types of resin were used, S-PRO (Sonnaya Ulitka S.L.), and 3DM-ABS (3D-Materials). Resin was poured on passive self-peeling (PSP) resin container, 3D printing was started once the building platform of the 3D printer touch down the PSP resin container. Exposure time depends on the resin type, 8 s from layer 1 to 2, and 4 s from layer 3 to 46 in case of S-PRO, and 4 s from layer 1 to 2, and 2 s from layer 3 to 46 in case of 3DM-ABS. The total height of both molds is 4.6 mm (layer 0 from the sketch is always deleted). The generated molds were immersed in isopropanol, shaken for 20 min at 24 °C, briefly washed with isopropanol, post-cured under UV-light (390 nm to 395 nm) with 20 W power for 4 hours at 24 °C, and finally incubated at 30 °C for 12 hours.

PDMS chip fabrication: After assembly (described in Figure 1), beach towel clips held the two structures together. The resulting mold was incubated in a 72 °C oven for 30 min and subsequently observed in a binocular to check whether the cylindrical part from the top mold touched the center of the channel part at the bottom mold. Meantime, polydimethylsiloxane (PDMS) precursor and a curing agent from Sylgard 184 Silicone Elastomer kit (Dow Corning) were mixed at a 9:1 ratio. After intensive mixing, the mixture was degassed under vacuum for

2 hours. The PDMS mixture was poured on the mold carefully avoiding air bubble formation, and cured at 72 °C for 50 min. The cured PDMS was gently detached from the mold (subsequently stored for another chip fabrication), dipped into acetone for 20 min, and into isopropanol for 10 min. After completely drying the cured PDMS, it was post-cured at 72 °C for 12 hours. At that point, the chip is a single-block PDMS containing two grooves that need to be sealed to form channels. An additional 10 mm x 3 mm x 5 mm (length x width x height) PDMS cube is used to cover the top channel. This cube is first punched with a 0.5 mm Biopsy Punch (World Precision Instruments) to create inlet and outlet holes. To glue the cube, a tiny amount of PDMS mixture is spread on the PDMS chip just around the top channel, the cube is placed over this liquid PDMS and the assembled blocks are cured at 72 °C for 30 min. A second 3 mm x 3 mm x 5 mm (length x width x height) PDMS cube is attached to the bottom inlet part in the same manner, a 0.5 mm Biopsy Punch is used to make a hole for inlet and outlet of the bottom channel. Finally, the bottom channel is sealed with a Precision Cover Glass #1.5 (Thorlabs) by plasma cleaner (Harrick Plasma) (Figure S1, Supporting Information). After incubation at 72 °C for 12 hours, squalene (ACROS Organics) was injected into each top and bottom channel for 10 mins to clean up inside of the chip. After washing with acetone and isopropanol for 5 mins and drying for at 24 °C for 2 hours, the chip is ready to use (Figure S1a, Supporting Information).

Bilayer formation from SUVs: The SUVs were prepared by sonication. Briefly, 5 mM lipids were dried and rehydrated with bilayer buffer (25 mM HEPES, 100 mM KCl, pH 7.4). The mixture was sonicated performing 3 times the continuous cycle, 5 s pulse and 5 s break for 4 minutes, with a pause of ~2 minutes between each cycle. The PDMS chip was filled with the lipid/squalene mixture, and two tubes containing bilayer buffer with SUV solution at 5 mM lipid were connected to the channels, one at the bottom inlet and the other at the top inlet, without any bubble inside. The chip was placed on the stage of Eclipse Ti confocal microscope (Nikon) with add-ons, including CSU-X spinning disk (Yokogawa), TuCam (Andor), dual iXon

Ultra camera (Andor), and EPC10 USB amplifier (HEKA) to which two electrodes inserted inside the top and bottom channels were connected. In the case of FRAP experiments, all this equipment, except Eclipse Ti Confocal microscope, was set up with a laser scanning confocal microscope (Leica-SP5). We used neMESYS Syringe Pumps (Cetoni) to accurately regulate the flow of up to 4 syringes separately. The syringe connected to the bottom channel pushed the bilayer buffer with 0.01 μl/s flow rate, then the other syringe was pushed in similar manner into the top channel just after the lipid monolayer formation at the surface between the buffer in the bottom channel and lipid/squalene at the hole. Once the electrodes were immersed with buffer, the buffer continuously flowed with 0.0012 μL/s in both channels. Bilayer formation was monitored both optically and electrically. Once the squalene droplet is formed between the channels, the bright-field images were recorded at 1 frame/s rate by the confocal microscope. Three types of objectives were used, 10x (NA 0.4 CFI Plan Apo Lambda), 20x free-immersion objective lens (NA 0.75, CFI S Fluor), 40x water-immersion objective (NA 1.15, CFI Apo Lambda S LWD 40XW), depending on the purpose of the experiment. Except for the FRAP experiment, all fluorophore was excited by either 488 nm laser or 640 nm laser incorporated in LU-N4 laser unit (Nikon). For the dual color imaging, images were split by 580 nm filter, and filtered either 525 nm or 679 nm, then recorded by each camera. At the same time, the capacitance was measured by the amplifier using silver chloride electrodes. A 10 mV sinusoidal wave with 20 kHz frequency was generated by the lock-in function controlled with the PatchMaster software provided by the amplifier manufacturer. Specific capacitance (C_S) of DOPC:DOPS:Chol:DOPE (35:10:25:30 mol%) bilayer was 7.5±0.4 mF/m^2 on average. Bilayer thickness was calculated as $d = \varepsilon_L\varepsilon_0/C_S \approx 3$ nm, we chose a 2.5 dielectric constant of bilayer (known to range between 2 and 3),[42, 43] and the vacuum permittivity is ~8.85 x 10^{-12} F/m. In the case of bilayer formation from lipid dissolved in squalene, ~2 mg/mL of lipids and squalene mixture was mixed and heated at 50 °C for 30 min, and at 24 °C for 12 hours. Then this mixture directly filled up the chip, and a tube containing the same buffer was connected.

When the bilayer forms, it spontaneously nucleates at a certain z-position within the cylindrical hole, usually close to the largest diameter of the quasi-cylindrical hole (Figure 1, and Figure S1, Supporting Information). If the exact position does not matter for the considered purpose, this is sufficient. In the case of the chip we present here, the diameter of the hole is slightly larger closer to the coverslip because of the 3D-printing. Hence the bilayer always forms closer to the coverslip which is an advantage in regards to the working distance of objectives. If a more precise positioning is required, conical shaped hole may be more appropriate but we did not test it. Also, having different flow rates in the two channels can help adjusting the z-position of the bilayer.

Protein purification: The t-SNARE complex composed of syntaxin1a and SNAP25 with all cysteines removed (and a single cysteine added at site Q20C of SNAP25) was purified as previously described.[44]

Protein labeling: The t-SNARE complex containing a single cysteine (Q20C) was labeled with ATTO 488-maleimide (ATTO TEC). For the immunofluorescence assay on the membrane, primary antibody, SMI 81 (Biolegend), was labeled with ATTO 488-NHS ester in 3:1 of dye:protein ratio. The fluorescence of each protein was measured by the spectrometer (SpectraMax M5, Molecular Devices) after free dye removal.

Proteo- membrane formation: Proteo-liposomes were used as carriers to transfer membrane proteins into the lipid bilayer. t-SNAREs were reconstituted into liposomes by the co-micellization method previously described. In brief, lipids (DOPC:DOPS:Cholesterol:DOPE with 35:10:25:30 in mol%) dried under argon and vacuum were rehydrated with bilayer buffer supplemented with 1 mM DTT and 1% n-octyl-β-D-glucoside (OG). The mixture was mixed with transmembrane proteins with lipid:protein ratio of 1:400 for 30 min at 24 °C, and rapidly diluted 3 times with bilayer buffer. The OG was removed by dialysis (10 kDa molecular weight cut-off) with the bilayer buffer containing 0.1% (w/v) of SM2 Biobead (Biorad) at 4 °C for 16 hours. The proteo-SUVs were collected by ultracentrifugation. First, they were mixed with the

same volume of 60% Optiprep, 20% and 0% of Optiprep mixture with the bilayer buffer were layered, respectively. After ultracentrifugation with 250,000 g at 4 °C for 5 hours, about 1.5 mM of proteo-SUV was collected between 20% and 0% layer. The reconstituted proteo-liposomes were analyzed by SDS-PAGE gel prior to the experiment to ensure the protein was incorporated. They were then introduced with an appropriate concentration (1 μM for immunofluorescence assay, 20 μM for FRAP) into the syringe tube that is subsequently connected to the top channel. After a squalene droplet is sandwiched between two monolayers, 3 μL of the proteo-SUV solution was flowed in the top channel at 0.02 μl/s flow rate. After the remaining unfused proteo-SUVs have been washed out, the signal from the fluorescently labeled protein or antibody was observed by confocal microscopy (in the case of antibody, it is flowed in similarly to the proteo-SUVs afterward, see Immunofluorescence assay below).

Fluorescence recovery after photobleaching: A laser scanning confocal microscope (Leica-SP5) equipped with a 488 nm argon laser was used for the fluorescence bleaching and recovery. Typically, each 512 x 512 pixels image was acquired in 0.67 s and represented a 150 μm x 150 μm area. The emitted light was collected by photomultiplier tubes from 520 nm to 600 nm wavelength, the laser power was automatically changed from 5% of the maximum power for pre- and post-bleaching to 100% with zoom-in the region of interest for a single bleaching scan. In Figure 6b (bottom), because the bleaching area is large (disk with a 95 μm diameter); ten bleaching scans with 100% laser power were used to ensure bleaching of the considered area.

Immunofluorescence assay on the free-standing membrane: To inject each component separately, one pump was used for injection into the bottom channel, and 3 pumps connected to 4-way junction were used for the top. Fluorescently labeled primary antibody, SMI 81 labeled with ATTO 488, and 10 ng/mL BSA was aspirated into the tube for the bottom channel injection, and one of the tubes for top channel injection. A secondary antibody labeled with Alexa Fluor 647 (Thermo Fisher Scientific), was aspirated into one of the tubes for the top channel injection.

Finally, 3 μl of 1 μM t-SUV were aspirated into the last tube for top channel injection. After the membrane containing t-SNAREs was formed, the primary antibody was injected either in the top or bottom channel at 0.01 μl/s for 20 min, followed by antibody-free buffer at 0.05 μl/s for 20 min. After the primary antibody was flown in the top-channel, the secondary antibody was injected at 0.01 μl/s for 20 min, followed by antibody-free buffer at 0.05 μl/s until the end of the experiment. During the antibody-free buffer washing step, each fluorophore was excited by both 488 and 640 nm, and dual color images were recorded.

Asymmetric bilayer formation: In total 4 lipid mixtures were prepared for 2 asymmetric bilayer formation. One set of lipid mixtures was made of brain extract (Porcine) and soy extract (Soybean). The other set of lipid mixtures contained, DOPC:DOPS:Chol:DOPE:PIP_2 with 5:10:50:30:5 (mol%), and DOPC:DOPS:Chol:DOPE:SM with 20:5:50:15:10 (mol%), mimicking respectively the inner and outer leaflet of a plasma membrane. To visualize the asymmetric bilayer formation, 2% of NBD-PE and 1% of ATTO 647N-DOPE was used instead of the equivalent amount of DOPE. These mixtures were dried under argon and vacuum, and rehydrated with bilayer buffer. To make SUVs, each rehydrated lipid mixture was sonicated and stored at 4 °C before usage. One tube for the top channel was filled with either brain extract or inner leaflet mimic SUVs, and the other tube for the bottom channel was filled with either soy extract of outer leaflet mimic SUVs. Squalene was trapped in the hole as described above. In case of visualization of an asymmetric bilayer, two tubes filled with 0.1 mM sodium dithionite were used for each top and bottom channel. After bilayer formation, sodium dithionite in the top channel was injected in 0.05 μl/s for 20 min, sodium dithionite in the bottom channel was injected in 0.05 μl/s until the end of the experiment. NBD (resp. ATTO 647N) was excited with 488 nm (resp. 640 nm) laser, and dual color images were recorded. As previously, the capacitance was recorded with a 10 mV sinusoidal wave at 20 kHz frequency.

α-hemolysin mediated current flow measurement: All α-hemolysin experiments were performed in hemolysin buffer (10 mM Tris-HCl, 1M KCl, 1 mM EDTA, pH 8.0). One tube was connected to the bottom channel and filled with hemolysin buffer. Two tubes, each attached to its own pump, were connected to the top channel with a t-shaped junction. The first one was filled up with hemolysin buffer and the other contained 3μL α-hemolysin (Sigma) at 40 nM. After bilayer formation, α-hemolysin was injected in 0.01 μl/s. The ionic current flow was measured by applying 50 mV voltage across the bilayer. The voltage-dependent current was measured with 25 mV step increase of voltage. In our setup, the current increases by 55 pA on average for a single hemolysin pore whose diameter was estimated by:

$$d = 2\sqrt{\frac{l\Delta I}{\pi GCU}}$$

Where d is the pore diameter, l the length of the channel (10 nm), ΔI the step increase in current (~55 pA), G the molar conductivity (~10 S/Mm), C the concentration (1 M) and U the voltage (50 mV).

In experiments where α-hemolysin was added when squalene was not yet fully absorbed by PDMS (blue dots in Figure 7h), the syringe connected to the top channel was filled with 3 μM α-hemolysin in hemolysin buffer. While the capacitance measurement of the sandwiched oil, the current was measured every 20 min with the same condition described above. Without α-Hemolysin, the difference of the measured current before and after bilayer formation was less than 4 pA.

PDMS chip regeneration: After each experiment, the PDMS chip was rinsed with acetone, distilled water, and isopropanol to remove remaining lipids, squalene, and buffer. It was then sonicated in a water bath to clean up the entire surface inside of the chip. Finally, the chip was dried for 2 hours dry at 24 °C, and ready to use again. The maximum number of reusing the PDMS chip was about 30 times. Usually, the total number of usages was defined by

spontaneous damage of the chip such as breakage of the hole for tube insertion, cover glass, and so on, rather than the life of PDMS.

Supporting Information

Supporting Information is available from the Wiley Online Library or from the author.

Acknowledgements

This work was supported by a European Research Council (ERC) funded grant under the European Union's Horizon 2020 research and innovation programme (grant agreement no. 669612) to J.E.R. JB. F. acknowledges funding from DFG grant SFB1027.

Received: ((will be filled in by the editorial staff))
Revised: ((will be filled in by the editorial staff))
Published online: ((will be filled in by the editorial staff))

References

1. J. Marra, *J Colloid Interf Sci* **1985,** *107* (2), 446-458. DOI Doi 10.1016/0021-9797(85)90197-3.
2. A. A. Brian; H. M. McConnell, *Proc Natl Acad Sci U S A* **1984,** *81* (19), 6159-63.
3. P. S. Cremer; S. G. Boxer, *J Phys Chem B* **1999,** *103* (13), 2554-2559. DOI DOI 10.1021/jp983996x.
4. F. Szoka, Jr.; D. Papahadjopoulos, *Annu Rev Biophys Bioeng* **1980,** *9*, 467-508. DOI 10.1146/annurev.bb.09.060180.002343.
5. N. Rodriguez; F. Pincet; S. Cribier, *Colloids Surf B Biointerfaces* **2005,** *42* (2), 125-30. DOI 10.1016/j.colsurfb.2005.01.010.
6. P. Mueller; D. O. Rudin; H. T. Tien; W. C. Wescott, *Nature* **1962,** *194*, 979-80.
7. M. Montal; P. Mueller, *Proc Natl Acad Sci U S A* **1972,** *69* (12), 3561-6.
8. M. H. Abdulreda; A. Bhalla; E. R. Chapman; V. T. Moy, *Biophys J* **2008,** *94* (2), 648-55. DOI 10.1529/biophysj.107.114298.
9. W. Hanke; C. Methfessel; U. Wilmsen; G. Boheim, *Bioelectroch Bioener* **1984,** *12* (3-4), 329-339. DOI Doi 10.1016/0302-4598(84)87013-0.
10. H. Bayley; B. Cronin; A. Heron; M. A. Holden; W. L. Hwang; R. Syeda; J. Thompson; M. Wallace, *Mol Biosyst* **2008,** *4* (12), 1191-208. DOI 10.1039/b808893d.
11. S. Ramakrishnan; A. Gohlke; F. Li; J. Coleman; W. Xu; J. E. Rothman; F. Pincet, *Langmuir* **2018,** *34* (20), 5849-5859. DOI 10.1021/acs.langmuir.8b00116.
12. L. Shi; Q. T. Shen; A. Kiel; J. Wang; H. W. Wang; T. J. Melia; J. E. Rothman; F. Pincet, *Science* **2012,** *335* (6074), 1355-9. DOI 10.1126/science.1214984.
13. K. Kamiya; R. Kawano; T. Osaki; K. Akiyoshi; S. Takeuchi, *Nat Chem* **2016,** *8* (9), 881-9. DOI 10.1038/nchem.2537.
14. M. Winterhalter, *Curr Opin Colloid In* **2000,** *5* (3-4), 250-255. DOI Doi 10.1016/S1359-0294(00)00063-7.
15. R. Coronado; R. Latorre, *Biophys J* **1983,** *43* (2), 231-6. DOI 10.1016/S0006-3495(83)84343-4.
16. L. L. Schwenen; R. Hubrich; D. Milovanovic; B. Geil; J. Yang; A. Kros; R. Jahn; C. Steinem, *Sci Rep* **2015,** *5*, 12006. DOI 10.1038/srep12006.
17. T. K. Ritchie; Y. V. Grinkova; T. H. Bayburt; I. G. Denisov; J. K. Zolnerciks; W. M. Atkins; S. G. Sligar, *Methods Enzymol* **2009,** *464*, 211-31. DOI 10.1016/S0076-6879(09)64011-8.
18. M. A. Schuler; I. G. Denisov; S. G. Sligar, *Methods Mol Biol* **2013,** *974*, 415-33. DOI 10.1007/978-1-62703-275-9_18.
19. P. Bartsch; C. Walter; P. Selenschik; A. Honigmann; R. Wagner, *Materials* **2012,** *5* (12), 2705-2730. DOI 10.3390/ma5122705.

20. V. C. Stimberg; J. G. Bomer; I. van Uitert; A. van den Berg; S. Le Gac, *Small* **2013,** *9* (7), 1076-1085. DOI 10.1002/smll.201201821.
21. H. Suzuki; K. V. Tabata; H. Noji; S. Takeuchi, *Biosens Bioelectron* **2007,** *22* (6), 1111-1115. DOI 10.1016/j.bios.2006.04.013.
22. P. J. Beltramo; R. Van Hooghten; J. Vermant, *Soft Matter* **2016,** *12* (19), 4324-4331. DOI 10.1039/c6sm00250a.
23. P. J. Beltramo; L. Scheidegger; J. Vermant, *Langmuir* **2018,** *34* (20), 5880-5888. DOI 10.1021/acs.langmuir.8b00837.
24. D. Marquardt; B. Geier; G. Pabst, *Membranes* **2015,** *5* (2), 180-196. DOI 10.3390/membranes5020180.
25. D. van Swaay; A. deMello, *Lab Chip* **2013,** *13* (24), 4890-4890.
26. R. Watanabe; N. Soga; T. Yamanaka; H. Noji, *Sci Rep-Uk* **2014,** *4*. DOI ARTN 7076 10.1038/srep07076.
27. C. M. Frey; H. Barth; C. Kranz; B. Mizaikoff, *Anal Methods-Uk* **2018,** *10* (26), 3153-3161. DOI 10.1039/c8ay01122b.
28. S. H. Wang; R. G. Larson, *Phys Chem Chem Phys* **2014,** *16* (16), 7251-7262. DOI 10.1039/c3cp55116d.
29. S. Shenoy; R. Moldovan; J. Fitzpatrick; D. J. Vanderah; M. Deserno; M. Losche, *Soft Matter* **2010,** *2010* (6), 1263-1274. DOI 10.1039/B919988H.
30. S. Purushothaman; J. Cama; U. F. Keyser, *Soft Matter* **2016,** *12* (7), 2135-2144. DOI 10.1039/c5sm02371h.
31. N. Malmstadt; M. A. Nash; R. F. Purnell; J. J. Schmidt, *Nano Lett* **2006,** *6* (9), 1961-5. DOI 10.1021/nl0611034.
32. B. Hille, *Ion channels of excitable membranes*. Sinauer: Sunderland, Mass., **2001**.
33. D. Johnston; S. M.-S. Wu, *Foundations of cellular neurophysiology*. MIT Press: Cambridge, Mass.; London, **1995**.
34. D. P. Nikolelis; U. J. Krull, *Talanta* **1992,** *39* (8), 1045-9.
35. N. Kahya; D. Scherfeld; K. Bacia; P. Schwille, *J Struct Biol* **2004,** *147* (1), 77-89. DOI 10.1016/j.jsb.2003.09.021.
36. L. Zhang; S. Granick, *J Chem Phys* **2005,** *123* (21), 211104. DOI 10.1063/1.2138699.
37. F. Pincet; V. Adrien; R. Yang; J. Delacotte; J. E. Rothman; W. Urbach; D. Tareste, *PLoS One* **2016,** *11* (7), e0158457. DOI 10.1371/journal.pone.0158457.
38. A. P. Pandey; F. Haque; J. C. Rochet; J. S. Hovis, *Biophys J* **2009,** *96* (2), 540-51. DOI 10.1016/j.bpj.2008.10.011.
39. R. Stefureac; Y. T. Long; H. B. Kraatz; P. Howard; J. S. Lee, *Biochemistry* **2006,** *45* (30), 9172-9. DOI 10.1021/bi0604835.
40. E. Evans; D. Needham, *J Phys Chem-Us* **1987,** *91* (16), 4219-4228. DOI DOI 10.1021/j100300a003.
41. G. A. Venkatesan; J. Lee; A. B. Farimani; M. Heiranian; C. P. Collier; N. R. Aluru; S. A. Sarles, *Langmuir* **2015,** *31* (47), 12883-12893. DOI 10.1021/acs.langmuir.5b02293.
42. J. P. Dilger; S. G. McLaughlin; T. J. McIntosh; S. A. Simon, *Science* **1979,** *206* (4423), 1196-8.
43. G. Gramse; A. Dols-Perez; M. A. Edwards; L. Fumagalli; G. Gomila, *Biophys J* **2013,** *104* (6), 1257-62. DOI 10.1016/j.bpj.2013.02.011.
44. T. Weber; B. V. Zemelman; J. A. McNew; B. Westermann; M. Gmachl; F. Parlati; T. H. Sollner; J. E. Rothman, *Cell* **1998,** *92* (6), 759-72.

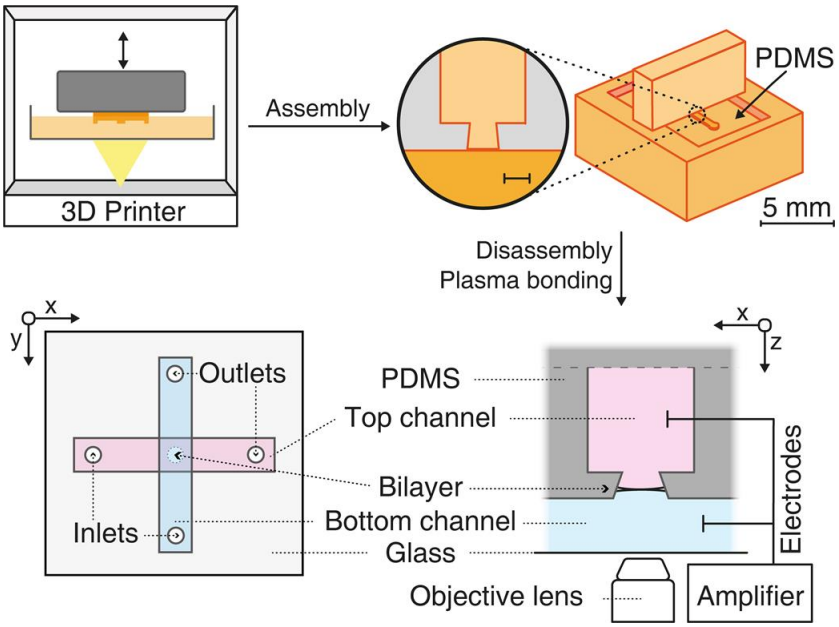

Figure 1. 3D printing-based microfluidic chip setup for performing optical and electrical measurements. The molds providing the top channel with a pillar to make the hole where the bilayer will be located and the bottom channel are produced by 3D-printer (top, left), then the PDMS mixture is casted on the assembled single mold (top, right). The final single-block microfluidic device contains two crossed channels (red and blue, bottom) separated by a hole where the horizontal free-standing bilayer will form (bottom). The process of bilayer formation and following assays can be simultaneously monitored by conventional apparatus, *e.g.* confocal microscopy and patch-clamp amplifier. Scale bar for inset is 100 µm.

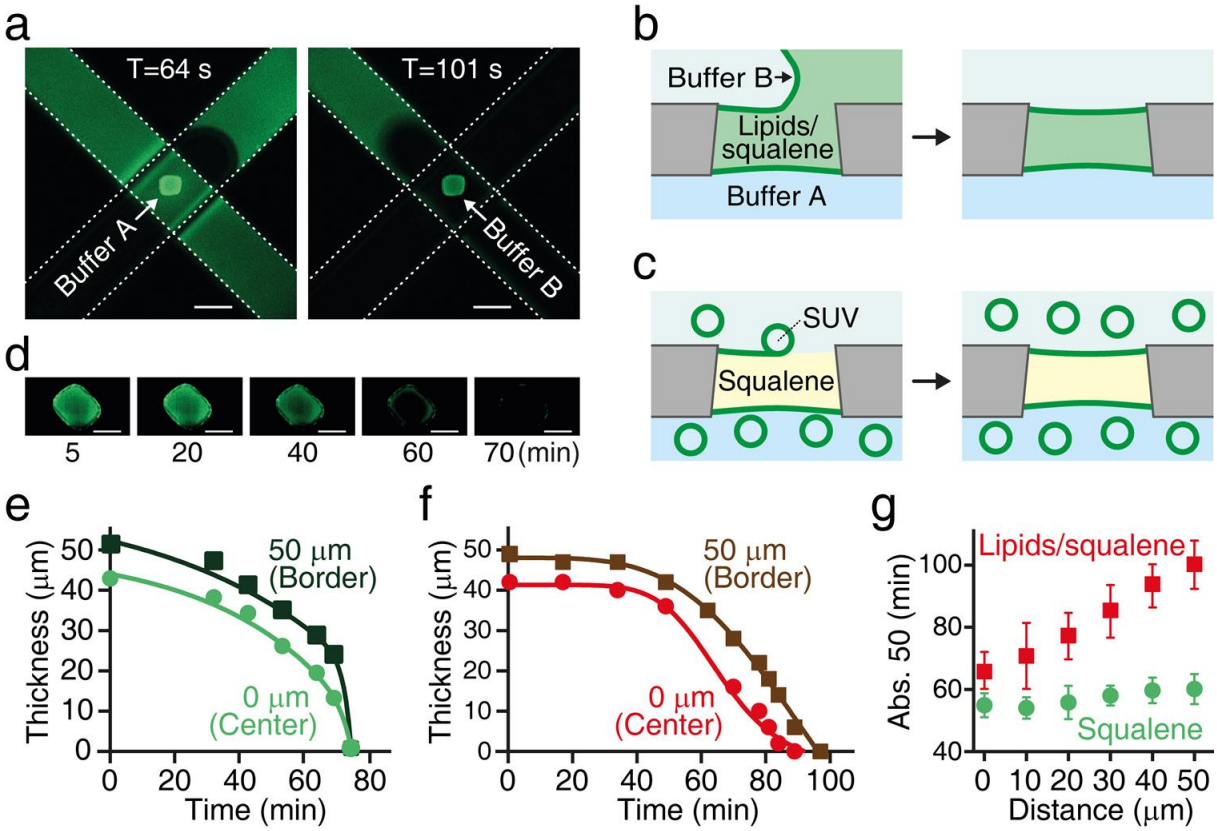

Figure 2. Trapping and absorption of a suspended squalene droplet sandwiched between two lipid monolayers in the hole. a) Lipid/squalene mixture (green) initially filling the chip is pushed away by a buffer at the bottom (left) and top (right) channels (Videos SV4 and SV5, Supporting Information). White dots indicate each channel. Scale bars, 200 μm. b,c) Two methods are available for lipid monolayer formation, b) lipid-in-oil or c) small unilamellar vesicles-on-oil: spontaneous spreading of liposome at the highly reactive interface between squalene and buffer. d) Fluorescence images of the squalene droplet (without lipids) being absorbed by the PDMS chip. Squalene was stained with BODIPY. Image at 70 min indicates a broken droplet allowing buffer connection between the two channels. Scale bar, 100 μm. e,f) Squalene droplet thinning e) without lipids or f) with lipids. Thickness of BODIPY-containing squalene was measured by z-stack images. g) 50% squalene thickness reduction time (Absorption 50) of PDMS from center (0 μm) to rim (50 μm) of the hole without (green) and with lipids (red). DOPC:DOPS:Cholesterol:DOPE (35:10:25:30 mol%) was used in f) and g).

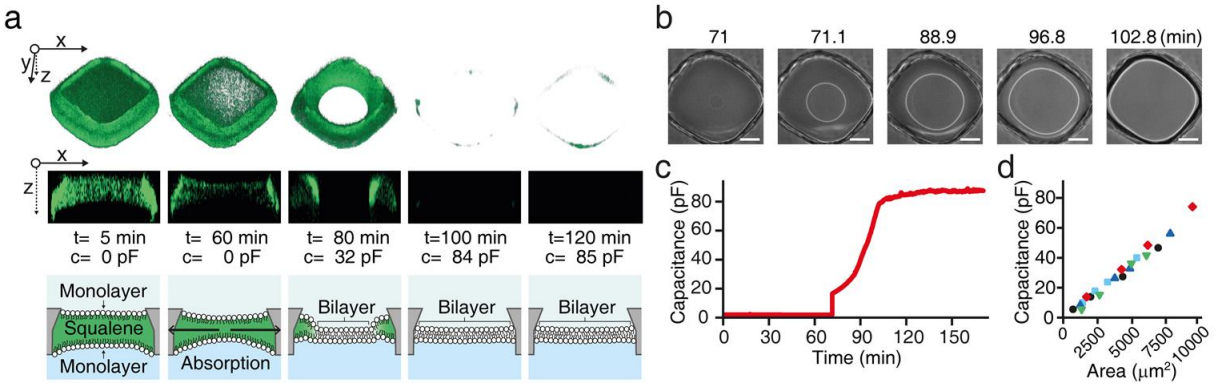

Figure 3. Simultaneous optical and electrical monitoring of bilayer formation. a) Tilted (top) and XZ projectin (middle) of time-dependent z-stack images, capacitance values across the channels and corresponding cartoon (bottom). The squalene droplet is labeled with BODIPY. t=80 min is just after bilayer nucleation. The fluorescence-free region inside of green area indicates the bilayer. The last two panels are during the capacitance plateau. Scale bars with arrows, 60 μm for x, y and 100 μm for z. b,c) Simultaneous observation of bilayer in b) bright-field and c) capacitance (Video SV1, Supporting Information). DOPC:DOPS:Cholesterol:DOPE (35:10:25:30 mol%) was used in this representative example. Scale bars in b), 25 μm. d) Bilayer area-dependent capacitance increase; the specific capacitance for the lipid composition presented in b) is 7.5±0.4 mF/m². Each symbol indicates independent measurements (5 in total). Error bars in the y-axis of each symbol are less than the symbol size.

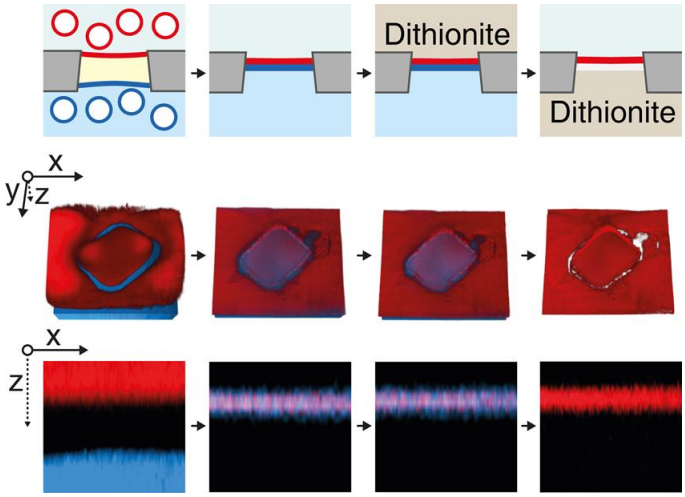

Figure 4. Formation of asymmetric bilayer with the SUVs-on-oil approach. Schematic illustration (top) and z-stack image for an asymmetric bilayer made of DOPC:DOPS:Cholesterol:DOPE:PIP_2:ATTO647N-DOPE (5:10:50:30:4:1 mol%) for top monolayer, DOPC:DOPS:Cholesterol:DOPE:Sphingomyelin:NBD-PE (20:5:50:13:10:2 mol%) for bottom monolayer. Dithionite quenches the fluorescent dye in the lower channel (NBD). NBD signal disappear only when dithionite is flowed in the lower channel, showing the asymmetry of the bilayer. Scale bars with arrows, 100 μm for x, y, z in the middle panel, and 50 μm for x and 100 μm for z in the bottom panels.

a

Lipids / mol%	Lifetime (min) Lipid-in-oil	Lifetime (min) SUVs-on-oil	%Increase
DOPC:DOPS:DOPE / 60:10:30	48±13	58±16	21
DOPC:DOPS:DOPE / 50:10:40	79±14	113±15	43
DOPC:DOPS:Chol:DOPE / 35:10:25:30	90±12	140±17	56
+ PIP_2 / 5	80±22	99±19	24
+ Cerebroside / 10	94±16	118±21	26
+ Sulfatide / 10	117±11	145±11	24
+ Sphingomyelin / 10	71±18	92±13	30
+ Chol / 25	159±10	167±13	5
Brain extract (Porcine)	95±14	120±22	26
Bacteria extract (*E. coli*)	113±15	150±19	33
Yeast extract (*S. cerevisiae*)	75±23	88±16	17
Liver extract (Bovine)	84±11	95±16	13
Heart extract (Bovine)	91±16	108±16	19
Soy extract (Soy bean)	103±17	140±27	36
Chimeric asymmetric bilayer Top monolayer Brain extract (Porcine) Bottom monolayer Soy extract (Soy bean)	-	174±17	-
Physiological asymmetric bilayer Top monolayer DOPC:DOPS:Chol:DOPE:PIP_2 / 5:10:50:30:5 Bottom monolayer DOPC:DOPS:Chol:DOPE:SM / 20:5:50:15:10	-	179±29	-

3 h
0 h

b

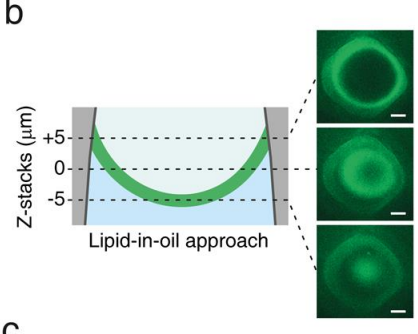

c

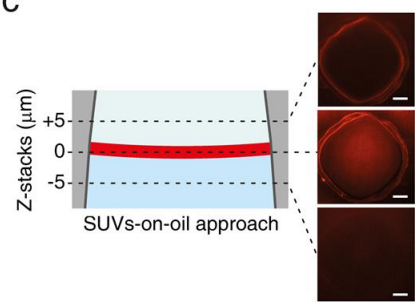

Figure 5. Stability and flatness of the membrane. a) Stability of symmetric and asymmetric bilayers with 16 lipid compositions. The first 14 compositions were equally made with both the lipid-in-oil or SUVs-on-oil approaches and reproducibly formed stable symmetric bilayers. The last two compositions formed stable asymmetric bilayers. They can only be done using the SUVs-on-oil approach. The lifetime of the bilayer is reported in the second column for the lipid-in-oil approach and the third column for membranes made from SUVs. The last column indicate the percentage of lifetime increase from lipid-in-oil to SUVs-on-oil. Chol and SM indicate cholesterol and sphingomyelin. Equivalent DOPC mol% from the 3rd lipid composition (DOPC, DOPS, Cholesterol, DOPE) is reduced when PIP_2, cerebroside, sulfatide, sphingomyelin, and more cholesterol was added separately. The success rate of membrane formation was close to 100%, omitting technical issues unrelated to the bilayer, including squalene absorption problem in newly made chip, damage on the connector for tube insertion, and so on. Typically, 10 membranes or more were tested in each case. b,c) Membrane flatness comparison of two bilayer forming strategies. After 90 minutes of bilayer formation with either b) lipid-in-oil or c) SUVs-on-oil protocol, z-stack fluorescence images were taken. Same lipid composition, DOPC:DOPS:Chol:DOPE:NBD-PE (34:10:25:30:1 mol%) was used in both cases. Scale bars, 25 μm. The number of trials for each case is indicated in Figure S3, Supporting information.

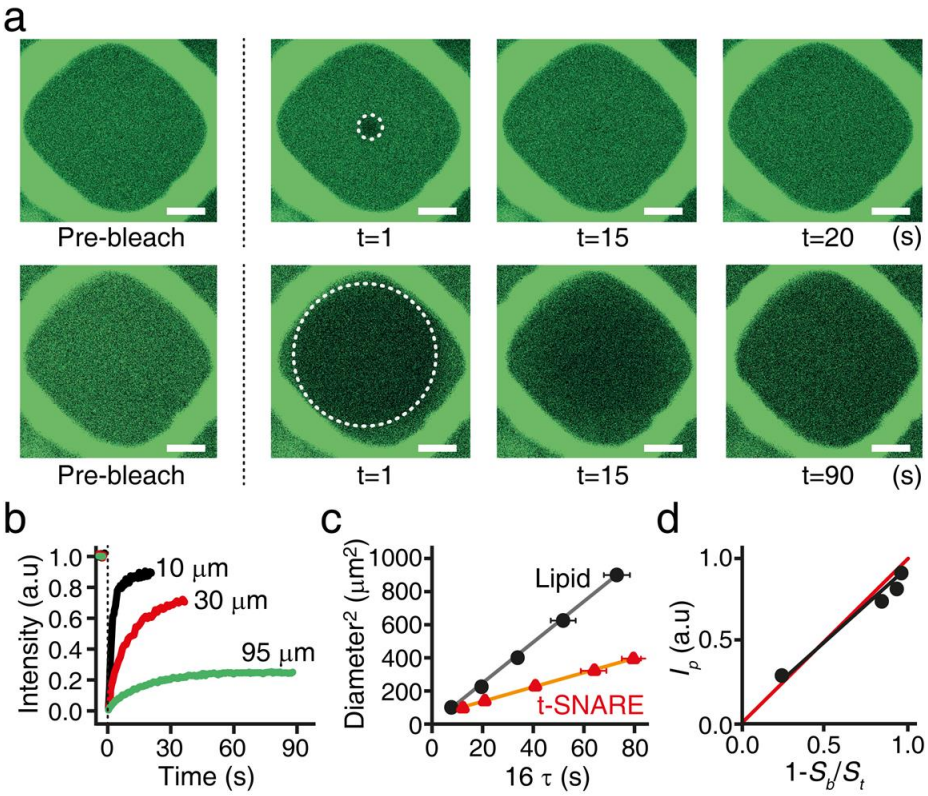

Figure 6. Fluorescence recovery after photobleaching of lipids in a bilayer. a) Representative recovery images of NBD-PE containing bilayer with 10 (top) or 95 μm (bottom) diameter bleached disk highlighted by the white dashed circle. Dashed line (black) indicates the beaching time. Scale bars, 25 μm. b) Fluorescence recovery with 10, 30, and 95 μm diameter bleached disks. c) Linear relationship between the recovery time and the bleached disk area. Disk diameter was 10, 12.5, 15, 20, 20.5, 30 μm for NBD-PE, and 10, 12.5, 15, 17.5. 20 μm for t-SNARE. Error bars at 10, 12.5, 15 μm disk diameter in all cases were less than the symbol dimension. d) Test of the relationship between the relative plateau intensity, I_p , in b) and the bleached disk area, S_p predicted by Eq. (1) and displayed as a red line. Error bars are less than the symbol.

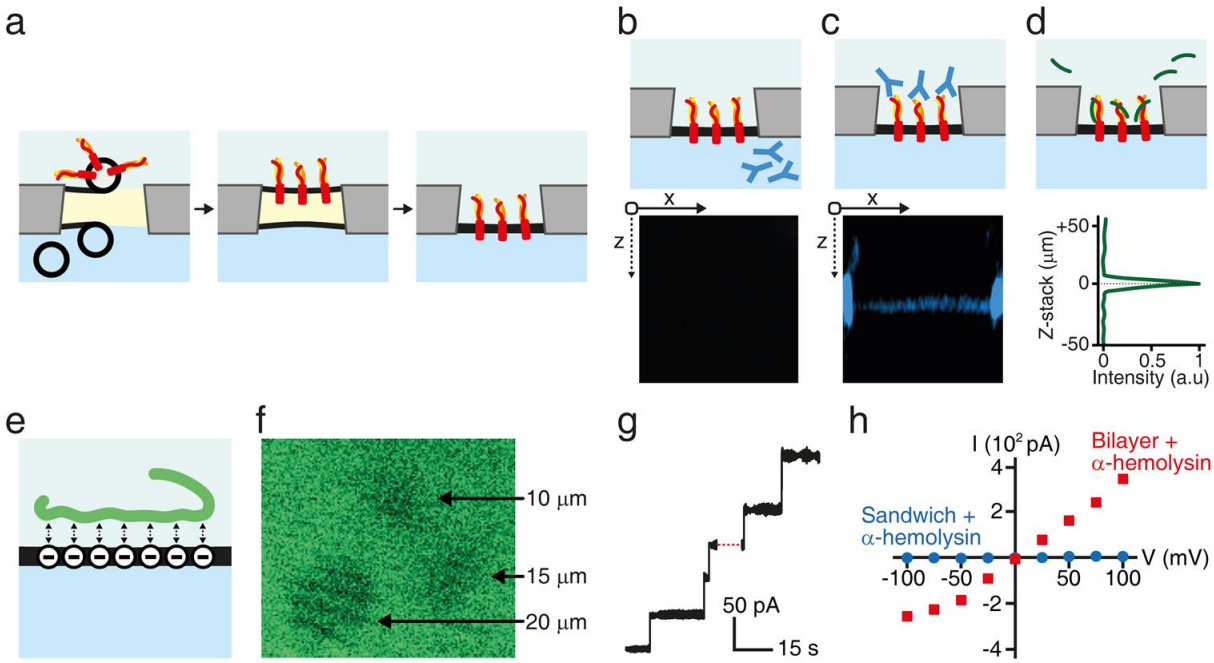

Figure 7. Characterization of membrane proteins. a) Protein inserting method into a free-standing bilayer adapting the SUVs-on-oil approach to proteo-SUVs. As an example, t-SNARE complex was used. b,c) Immunofluorescence assay for orientation analysis. Fluorescently labeled primary antibody (blue) is injected into the b) bottom channel, and c) top channel in sequential manner after t-SNARE incorporation into a bilayer. The top cartoons sketch the experiment and the lower images show the final intensity of the membrane after rinsing off the antibodies. Scale bars, 50 µm for x, z. d) schematic illustration of functionality assay. The cognate binding pair, CTD of v-SNARE, was labeled with ATTO-550 and injected to the top channel. The lower graph shows the intensity projection of ATTO-550 labeled CTD of v-SNARE; in z-axis, 0 µm indicates the focal plane position of the bilayer. e) Schematic illustration of interactions between α-Synuclein (green) and negatively charged bilayer. f) Zoom in on a DOPC:DOPC:Chol:DOPE (35:10:25:30 mol%) membrane with bound fluorescent α-Synuclein. Five minutes after 3 successive FRAP experiments with 10, 15 and 20 µm bleached disks respectively, the patterns of the disks are still visible showing that α-Synuclein is immobile. g) α-Hemolysin at 40 nM in 10 mM Tris-HCl, 1M KCl, 1 mM EDTA, pH 8.0 spontaneously forms channels that are observed by jumps in current under a constant 50 mV tension applied between the two sides of the bilayer. h) Current-voltage characteristics of α-hemolysin channels. Blue circles were obtained when a thick squalene droplet was still separating the two leaflets and red squares were measured after bilayer formation, by varying the tension during the red dashed section in g).

Supporting text

Supporting File 1

Click here to access/download

Supporting Information

SF1_3D Sketch.dwg

Supporting File 2

Click here to access/download

Supporting Information

SF2_3D mold_Bottom.stl

Supporting File 3

Supporting Video 1

Click here to access/download
Supporting Information
SV1_Sandwich_488nm.avi

Supporting Video 2

Click here to access/download
Supporting Information
SV2_Sandwich_BF.avi

Supporting Video 3

Click here to access/download
Supporting Information
SV3_Circular bilayer.avi

Supporting Video 4

Click here to access/download
Supporting Information
SV4_Triangle bilayer.avi

Supporting Video 5

Click here to access/download
Supporting Information
SV5_Rectangular bilayer.avi

Supporting Video 6

Click here to access/download
Supporting Information
SV6_Swelling.avi

Bottom mold slice

Bottom mold slice

Bottom mold slice

Bottom mold slice

Bottom mold slice

Bottom mold slice

Bottom mold slice

Bottom mold slice

Bottom mold slice

Bottom mold slice

Bottom mold slice

Bottom mold slice

Bottom mold slice

Bottom mold slice

Bottom mold slice

Bottom mold slice

Bottom mold slice

Bottom mold slice

Bottom mold slice

Bottom mold slice

Bottom mold slice

Bottom mold slice

Bottom mold slice

Bottom mold slice

Bottom mold slice

Bottom mold slice

Bottom mold slice

Bottom mold slice

Bottom mold slice

Bottom mold slice

Bottom mold slice

Bottom mold slice

Bottom mold slice

Bottom mold slice

Bottom mold slice

Bottom mold slice

Bottom mold slice

Bottom mold slice

Bottom mold slice

Bottom mold slice

Bottom mold slice

Bottom mold slice

Bottom mold slice

Bottom mold slice

Bottom mold slice

Bottom mold slice

Top mold slice

Top mold slice

Top mold slice

Top mold slice

Top mold slice

Top mold slice

Top mold slice

Top mold slice

Top mold slice

Top mold slice

Top mold slice

Top mold slice

Top mold slice

Top mold slice

Top mold slice

Top mold slice

Top mold slice

Top mold slice

Top mold slice

Top mold slice

Top mold slice

Top mold slice

Top mold slice

Top mold slice

Top mold slice

Top mold slice

Top mold slice

Top mold slice

Top mold slice

Top mold slice

Top mold slice

Top mold slice

Top mold slice

Top mold slice

Top mold slice

Top mold slice

Top mold slice

Top mold slice

Top mold slice

Top mold slice

Top mold slice

Top mold slice

Top mold slice

Top mold slice

Top mold slice

Top mold slice

Table of Content Image